Emission of plasmons by drifting Dirac electrons: A hallmark of hydrodynamic transport

Dmitry Svintsov *

Laboratory of 2d Materials for Optoelectronics, Moscow Institute of Physics and Technology, Institutsky lane 9, Dolgoprudny 141700, Russia

(Received 8 August 2019; revised manuscript received 14 October 2019; published 25 November 2019)

Direct current in clean semiconductors and metals was recently shown to obey the laws of hydrodynamics in a broad range of temperatures and sample dimensions. However, the determination of frequency window for hydrodynamic phenomena remains challenging. Here, we reveal a phenomenon being a hallmark of high-frequency hydrodynamic transport, the Cerenkov emission of plasmons by drifting Dirac electrons. The effect appears in a hydrodynamic regime only due to reduction of plasmon velocity by electron-electron collisions below the velocity of carrier drift. To characterize the Cerenkov effect quantitatively, we analytically find the high-frequency nonlocal conductivity of drifting Dirac electrons across the hydrodynamic-to-ballistic crossover. We find the growth rates of hydrodynamic plasmon instabilities in two experimentally relevant setups: parallel graphene layers and graphene covered by subwavelength grating, further showing their absence in ballistic regime. We argue that the possibility of Cerenkov emission is linked to singular structure of nonlocal conductivity of Dirac materials and is independent on specific dielectric environment.

DOI: 10.1103/PhysRevB.100.195428

I. INTRODUCTION

The realm of hydrodynamic transport spans at length scales exceeding the particle free path [1]. Experimental demarcation of hydrodynamics and ballistics is conveniently performed by measuring the flow through a pipe between two reservoirs. The flow through wide pipes is limited by viscosity (Poiseuille flow), while in narrower pipes it is limited by particle injection (Knudsen flow). Recently, similar experiments were performed in ultraclean solid-state systems, including thin metal wires [2], Weyl semimetals [3], GaAs-based quantum wells [4], and graphene [5–7]. They have revealed quite a broad window of temperatures and sample dimensions where electrons obey the laws of hydrodynamics [8] but not ballistics, as thought previously [9].

While the place for dc hydrodynamic (HD) phenomena on temperature and length scales is established [10,11], the bounds for hydrodynamics on the frequency scale are less probed [12]. Generally, electron-electron (e-e) collisions being the prerequisite of HD transport affect neither dc nor ac conductivity in *uniform* fields, though they may affect the properties of waves in solids—plasmons. Still, the spectra of plasmons in HD and ballistic regimes are almost identical as they are dictated by long-range Coulomb forces insensitive to microscopic details of e-e interactions [13,14]. The character of damping due to e-e scattering in ballistic and HD regimes is different [15,16], still it is often masked by extrinsic damping.

In this paper, we theoretically reveal a plasmonic phenomenon serving as a hallmark of hydrodynamic transport which is fully prohibited in a collisionless ballistic regime. The effect is emission of plasmons by drifting Dirac electrons or, in other words, Cerenkov plasmon instability of electron drift. Our emphasis on Dirac electron systems, especially graphene, is motivated by numerous observations of hydrodynamic phenomena therein [5–7,17], though some fingerprints of effect can be found in systems of massive electrons.

The possibility of Cerenkov instability in the HD regime is not merely due to reduction of viscous dissipation. It appears due to softening of plasmon velocity by e-e collisions down to the value sufficient to provide phase synchronism between drifting carriers and waves. More precisely, the lower bound on ballistic plasmon velocity in materials with Dirac spectra $\epsilon_p = \pm p v_0$ is exactly the carrier velocity v_0 [18,19]. The velocity of drift $u_0 < v_0$ thus never satisfies the Cerenkov criterion. In the HD regime, the lower bound on plasmon velocity is only $v_0/\sqrt{D}$, where D is the dimension of space [16,20]. The carriers accelerated to drift velocity $u_0 > v_0/\sqrt{D}$ are thus capable of plasmon emission.

The current-driven plasmon emission in graphene-based systems was already studied in Refs. [21,22]. Unfortunately, these studies (being limited to a collisionless regime) ignored the important issue of broken Galilean invariance in Dirac systems [23]. This breakdown makes the Doppler transform inapplicable for prediction of plasmon frequencies in a moving reference frame [24,25]. As argued in our recent Comment [26], this fact fully suppresses the Cerenkov plasmon emission in graphene double layers in the ballistic regime. More accurate studies [27–29] revealed no Cerenkov-type instabilities in graphene-based systems but were limited to the collisionless case [30].

Below we construct the theory of plasmon instabilities in Dirac systems that can handle the subtle issues of Galilean invariance breakdown. Moreover, it is possible to trace the evolution of instabilities across the hydrodynamic-to-ballistic crossover *analytically*. It is based on the solution of a kinetic equation with model e-e collision integral satisfying the conservation laws [13–16]. The obtained conductivity $\sigma(q, \omega)$ of drifting Dirac electrons has a number of unexpected features,

* svintcov.da@mipt.ru

 ©2019 American Physical Society

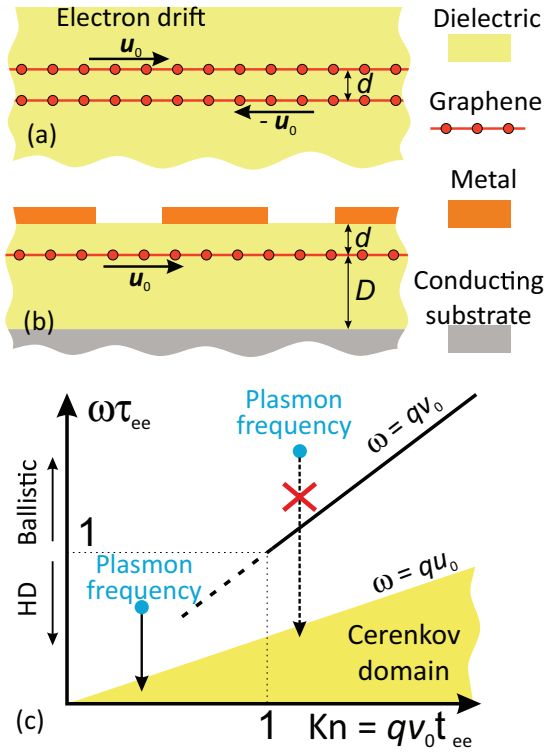

FIG. 1. Two possible graphene-based setups where hydrodynamic plasmon instabilities can be observed: (a) parallel layers with counterstreaming electrons with velocities $\pm u_0$, (b) graphene covered with subwavelength plasmonic grating and a highly-conducting substrate, and (c) schematic of changes in plasmon frequency (blue circles) with increasing drift velocity u_0 in Dirac materials at different Knudsen numbers $\mathrm{Kn} = qv_0\tau_{ee}$. Black solid line shows the position of singularity in ballistic nonlocal conductivity. The singularity becomes softer (dashed black line) in the hydrodynamic regime.

including the absence of dissipation at special frequencies and wave vectors satisfying $\omega u_0 = qv_0^2$. It is subsequently used as a building block for analysis of current-driven plasmon instabilities in experimentally relevant setups, including parallel graphene layers and graphene covered by subwavelength gratings, shown in Figs. 1(a) and 1(b).

The unstable plasmon modes in nonequilibrium systems can emerge, generally, in two ways. First, the plasmon gain can gradually transform into loss without an appreciable modification of resonant frequency. Such a situation is common for plasmons bound to conductors embedded in gain medium, as the degree of population inversion in that medium is gradually increased [31]. Second, the instability can emerge upon coalescence of modes with positive and negative real frequencies. Such a situation is common for waves in countersteaming flows [32,33]. For any of these instabilities, the plasmon frequency should reach (at least) the region of Cerenkov emission $\omega < qu_0$. We shall see that it is impossible for plasmons in 2D Dirac materials in the ballistic regime, as the material conductivity is singular at $\omega = qv_0 > qu_0$, as shown in Fig. 1(c). The singularity is washed out in the hydrodynamic regime, which gives way to possible instabilities.

II. CONDUCTIVITY OF DRIFTING DIRAC ELECTRONS AT THE HYDRODYNAMIC-TO-BALLISTIC CROSSOVER

The conductivity $\sigma(q,\omega)$ of drifting Dirac electron fluid is obtained by solving the kinetic equation for distribution function $f_{\mathbf{p}} = f_{\mathbf{p}}^{(0)} + \delta f_{\mathbf{p}}$ within a linear response to the external electric field $\delta \mathrm{E}_{\mathbf{q}} = -i\mathbf{q}\delta\varphi_{\mathbf{q}} e^{i(\mathbf{qr}-\omega t)}$:

$$-i\omega\delta f_{\mathbf{p}} + i\mathbf{q}\mathbf{v}_{\mathbf{p}}\delta f_{\mathbf{p}} + i\mathbf{q}\delta\varphi_{\mathbf{q}}\partial_{\mathbf{p}} f_{\mathbf{p}}^{(0)} = \mathcal{C}_{ee}\{\delta f_{\mathbf{p}}\}, \tag{1}$$

here $\mathbf{v}_{\mathbf{p}} = \partial_{\mathbf{p}}\epsilon_{\mathbf{p}}$ is the quasiparticle velocity. The carrier drift is encoded in a zero-order distribution function, which we take in the local-equilibrium (hydrodynamic) form with velocity $\mathbf{u}_0$, Fermi energy μ, and temperature T, $f_0 = [1 + e^{(\epsilon_p - \mathbf{p}\mathbf{u}_0 - \mu)/T}]^{-1}$. We restrict ourselves to collinear propagation of waves and carrier drift.

The crucial step of the solution is the approximation of e-e collision integral $\mathcal{C}_{ee}\{\delta f_{\mathbf{p}}\}$ which does not enable any analytical treatment in its original form. We adopt $\mathcal{C}_{ee}\{\delta f_{\mathbf{p}}\}$ that pulls all perturbations of distribution function toward a local equilibrium δf_{hd} (but not to zero [13,34]) with a characteristic rate $\gamma_{ee} = \tau_{ee}^{-1}$:

$$\mathcal{C}_{ee}\{\delta f_{\mathbf{p}}\} = -\gamma_{ee}(\delta f_{\mathrm{p}} - \delta f_{\mathrm{hd}}), \tag{2}$$

$$\delta f_{\mathrm{hd}} = \delta\mu\partial_\mu f_{\mathbf{p}}^{(0)} + \delta\mathbf{u}\partial_{\mathbf{u}} f_{\mathbf{p}}^{(0)} + \delta T\partial_T f_{\mathbf{p}}^{(0)}. \tag{3}$$

The main properties of true e-e scattering are encoded into the model, as the distribution modes corresponding to shift of particle number, momentum, and energy are not relaxed. The weights of these modes $\delta\mu$, $\delta\mathbf{u}$, and δT are obtained from respective conservation laws for e-e collisions. These requirements lead us to a linear system of generalized HD equations which can be written symbolically as $\hat{M}\delta\mathbf{x} = \delta\mathbf{F}$. The vector $\delta\mathbf{x}$ contains unknown hydrodynamic parameters that can be arbitrary linear combinations $\delta\mu$, δu, and δT; $\delta\mathbf{F}$ is the vector of generalized force densities, and $\hat{M}$ is the dynamic matrix. The simplest form is achieved when relative perturbations of particle density $\delta n/n_0$, 'relativistic' velocity $\delta\beta = \delta u/v_0$, and mass density $\delta\rho/\rho_0$ are treated as unknowns. In this representation, the HD matrix and force vector take the form (Supplemental Material, Sec. I and II [35])

$$\hat{M} = \begin{pmatrix} 1 - i\tilde{\gamma}_{ee}I_{02} & -i\tilde{\gamma}_{ee}\partial_\beta I_{02} & 0 \\ 0 & 1 - \frac{2}{3}i\tilde{\gamma}_{ee}\partial_\beta I_{13} & \beta_0 - \frac{2}{3}i\tilde{\gamma}_{ee}I_{13} \\ 0 & \beta - i\tilde{\gamma}_{ee}\partial_\beta I_{03} & 1 + \frac{\beta^2}{2} - i\tilde{\gamma}_{ee}I_{03} \end{pmatrix} \tag{4}$$

$$\delta\mathbf{F} = -2\frac{e\delta\varphi}{mv_0^2}\begin{pmatrix} I_{12} - \beta_0 I_{02} \\ I_{23} - \beta_0 I_{13} \\ \frac{3}{2}(I_{13} - \beta_0 I_{03}) \end{pmatrix} \tag{5}$$

where we have introduced 'relativistic mass' $m \approx \mu/v_0^2$, the inverse Knudsen number $\tilde{\gamma}_{\mathrm{ee}} = (qv_0\tau_{\mathrm{ee}})^{-1}$, and dimensionless functions $I_{nm}(a,\beta)$ of scaled frequency $a = (\omega + i\gamma_{ee})/qv_0$ and drift velocity β (closed-form expressions are given in Supplemental Material Sec. III [35]):

$$I_{nm}(a,\beta) = \frac{(1-\beta^2)^{m-\frac{1}{2}}}{2\pi}\int_0^{2\pi}\frac{\cos^n\theta d\theta}{(1-\beta\cos\theta)^m(a-\cos\theta)}. \tag{6}$$

The system (4) and (5) is the central result of this paper. It provides an explicit expression for high-frequency nonlocal graphene conductivity $\sigma(\mathbf{q}, \omega)$ in the presence of carrier drift across the hydrodynamic-to-ballistic crossover (Supplemental Material, Sec. II [35]). It encloses numerous previous studies of graphene ac conductivity as limiting cases [16,36,37]. Particularly, classical Navier-Stokes equations along with microscopic expression for viscosity are restored in the HD limit $\tilde{\gamma}_{ee} \gg 1$ by expanding I_{nm}. The polarization function in this limit reads as

$$\Pi_{\rm hd} = -\frac{nq^2(1-\beta_0^2)/m}{\omega^2(1-\beta_0^2/2) - \frac{q^2v_0^2}{2}(1-2\beta_0^2) - 2qu_0\omega}. \quad (7)$$

In the absence of current it acquires the common [38–40] hydrodynamic form

$$\Pi_{\rm hd}(\beta_0 = 0) = -\frac{nq^2/m}{\omega^2 - v_s^2q^2}, \quad (8)$$

where $v_s = v_0/\sqrt{2}$ is the sound velocity. The result (8) is not specific to graphene and coincides with that for massive two-dimensional electrons in the $T = 0$ limit [39]. This is not surprising due to formal coincidence of linearized hydrodynamic equations in these two systems at $\beta_0 = 0$, after the 'carrier mass' in graphene is properly defined. Important distinctions between graphene and massive 2D electrons appear in the presence of drift due to the breakdown of Galilean invariance.

In the ballistic limit, $\tilde{\gamma}_{ee} \ll 1$, the polarization of drifting graphene electrons becomes [26,36]

$$\Pi_{\rm bal} = \frac{2}{\pi}\frac{|\mu|/\hbar^2v_0^2}{(1-\omega u_0/qv_0^2)^2}\left(\sqrt{1-\beta_0^2} - \frac{\omega/qv_0 - \beta_0}{\sqrt{(\omega/qv_0)^2-1}}\right). \quad (9)$$

It coincides with the polarization found in Refs. [41,42] in the absence of drift and in the classical limit ($\hbar\omega \ll |\mu|$, $q \ll k_F$). The breakdown of Galilean invariance is even more pronounced in the ballistic case; indeed, the strong square-root singularity in the polarizability at $\omega = qv_0$ is insensitive to carrier drift. This singularity prevents the appearance of plasmon modes with frequencies below qv_0, as recently shown experimentally [19].

The system of equations (4) and (5) enables us to track the transformation of ballistic polarization (9) into a hydrodynamic one (7) by increasing the strength of e-e collisions and to study the possible plasmon instabilities at arbitrary frequencies.

III. DRIFT-INDUCED DOPPLER SHIFT AND PLASMON UNDAMPING

Several nontrivial plasmonic effects appear already in the isolated graphene layer in the presence of drift due to the breakdown of Galilean invariance. The latter is readily seen from the generalized hydrodynamic system (4) and (5) as the wave frequency ω and drift velocity u_0 appear therein not only in combination $\omega - qu_0$, as it should be for massive electrons.

The first such effect is anomalous Doppler splitting between frequencies of up- and downstream plasmons $\Delta\omega^{\pm}$. It is always below the conventional value of $2qu_0$; in the hydrodynamic limit it is exactly one half of it. In the ballistic limit

$$\Delta\omega^{\pm}_{\rm bal} = 2qu_0(s^2-1)(\sqrt{s^2-1} - s)^2, \quad (10)$$

where $s = \omega/qv_0$ is the ratio of wave phase velocity and Fermi velocity. The ballistic Doppler shift approaches zero as the wave velocity approaches v_0; it stems from singular ballistic conductivity at $\omega = qv_0$.

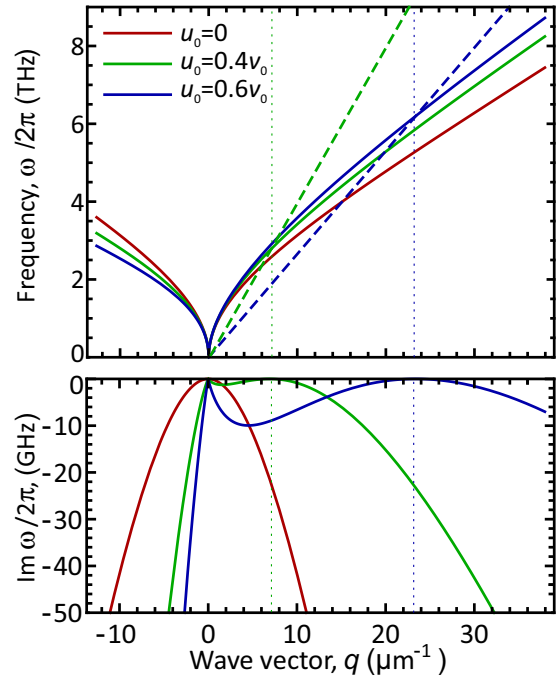

FIG. 2. Plasmon spectra (top) and damping (bottom) in a single graphene layer in the presence of e-e collisions at different drift velocities. Positive wave vectors correspond to waves co-propagating with drift. Damping disappears at $q = 0$ and $\omega u_0 = qv_0^2$ (the latter set of frequencies and wave vectors is marked with dashed lines). Fermi energy $\mu = 25$ meV, background dielectric constant $\kappa = 5$, scattering rate $\gamma_{ee} = 6 \times 10^{12}$ s^{-1}.

Much more surprising is the wave damping due to e-e collisions, which is shown in the bottom panel of Fig. 2. The damping of the upstream wave continuously increases with the drift speed. The damping of the downstream wave for finite u_0 approaches zero at some peculiar frequencies satisfying $\omega u_0 = qv_0^2$ and then continues to grow. Far away from the 'undamping point,' the imaginary part of frequency is proportional to q^2, as it should be for the viscous damping.

The origin of undamping points can be traced back to the excitation of distribution modes δf that are insensitive to e-e collisions. This is readily seen in 'boosted coordinates' $(\tilde{p}, \theta)$, where $\tilde{p} = p(1 - \beta\cos\theta)$ [43]. In the absence of collisions and at $T/\mu \ll 1$, an electric field excites the distributions

$$\delta f \propto \frac{\cos\theta\,\delta(\tilde{p}v_0 - \mu)}{[1-(qv_0/\omega)\cos\theta][1-\beta\cos\theta]^2}, \quad (11)$$

which do not generally coincide with zero modes of $\mathcal{C}_{ee}$ and are therefore relaxed. But at special points $qv_0/\omega = \beta$, the excited distribution coincides with the hydrodynamic

momentum mode of C_{ee}:

$$\delta f \propto \frac{\cos\theta\,\delta(\tilde{p}v_0 - \mu)}{[1-\beta\cos\theta]^3}. \tag{12}$$

It implies that collisions do not have any effect on these modes, and relaxation is absent. We note here that undamping occurs not only for plasmons, but the whole conductivity becomes dissipationless ($\sigma'(q,\omega)=0$) at these special frequencies and wave vectors.

IV. INSTABILITIES OF COUNTERSTREAMING FLOWS

Cerenkov-type plasmon instability is most simply achieved in a double layer setup where electron velocities in two layers point in the opposite direction. The theory of such instabilities developed for massive electrons [32] was recently erroneously applied to graphene in the ballistic regime [21,22]. Here, we find that the very presence of such instabilities depends strongly on the transport regime in the two layers.

Some hints on the possible instabilities in the double-layer system can be foreseen already from analysis of plasmon dispersion *in the absence* of direct current. In the ballistic regime $\omega\tau_{ee} \gg 1$, the system supports optical (+) and acoustic (−) plasmon modes with dispersions [44]

$$\omega^{\pm}_{\rm bal}(\beta_0=0) = v_0 q \frac{1+2K(1\pm e^{-|q|d})}{\sqrt{1+4K(1\pm e^{-|q|d})}}, \tag{13}$$

where $K = 2\alpha_c k_F/q$ is the dimensionless 'mode stiffness' and $\alpha_c = e^2/\kappa\hbar v_0$ is the Coulomb coupling constant. Naturally, even the lowest-frequency acoustic mode (13) has the phase velocity exceeding Fermi velocity v_0 and cannot be pulled by the current to the Cerenkov gain region. On the contrary, the plasmon frequencies in the hydrodynamic regime $\omega\tau_{\rm ee}$ are softer and given by

$$\omega^{\pm}_{\rm hd}(\beta_0=0) = v_0 q\sqrt{\frac{1}{2}+K(1\pm e^{-|q|d})}. \tag{14}$$

Here, the lower bound of plasmon velocity is $v_0/\sqrt{2}$, and it can potentially interact with drifting carriers.

The above suggestions are fully supported by analysis of plasmon modes with full polarizability of graphene electrons in the presence of current (Supplemental Material, Sec. IV [35]). The symmetric (optical) plasmon mode is unaffected by drift, while the frequency of the asymmetric one is pulled by current toward lower frequencies. However, it cannot be decreased below the boundary of single-particle excitations $\omega = qv_0$ due to the singular nonlocal response of graphene, as given by Eq. (10). As a result, the gain region encloses no plasmon eigenmode.

The acoustic mode, however, readily reaches the region of the Cerenkov gain in the hydrodynamic regime, as shown in Fig. 3(a). The nonlocal dielectric response of graphene in this regime is no more singular, and the wave frequency unimpededly passes through the $\omega = qv_0$ border. Above the critical velocity, the mode aperiodically growing, i.e., $\mathrm{Im}\omega > 0$, $\mathrm{Re}\omega = 0$. The range of velocities for observation of

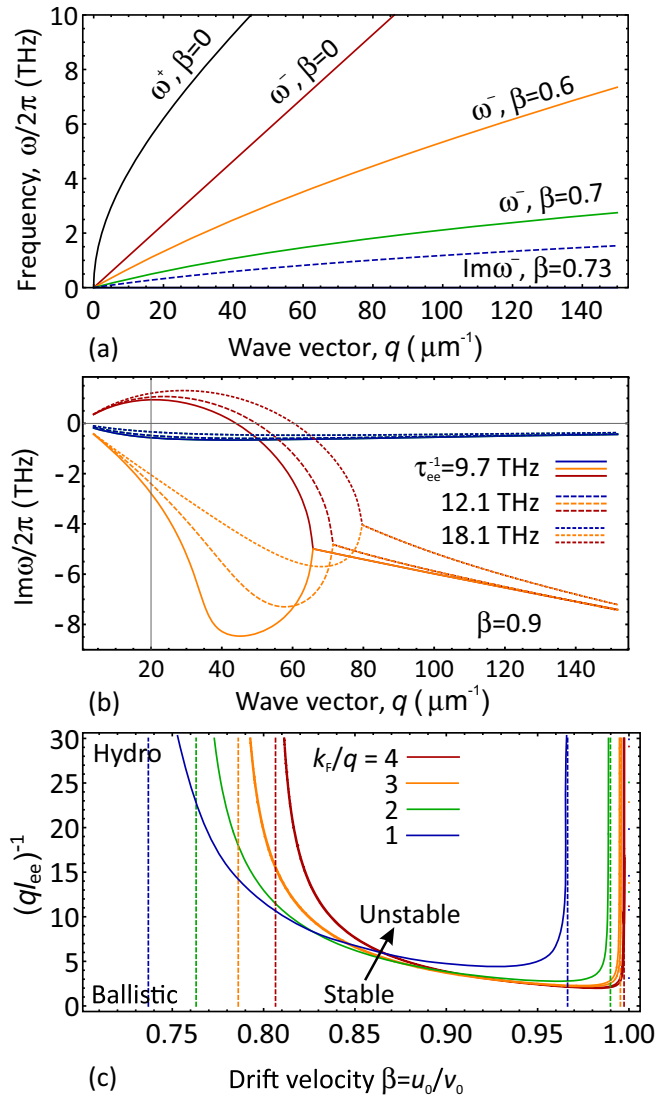

FIG. 3. Plasmons in graphene double layers with counterstreaming flows (a) Evolution of plasmon spectra in HD regime with increasing drift velocity β leading to the shift of acoustic mode frequency down to zero and subsequent instability (b) Damping/growth rates of plasmons at different values of e-e scattering rate, demonstrating suppression of instability with reduced scattering. Blue line corresponds to damping of optical mode being (almost) insensitive to drift; orange and dark red lines show the damping/gain of a couple of acoustic modes (c) Stability diagram of the double-layer setup: critical value of velocity and inverse Knudsen number at which plasma waves become unstable. Dashed lines in (c) are critical velocities calculated using Eq. (15). In panels (a) and (b), interlayer distance $d = 1$ nm, Fermi energy $\mu = 25$ meV. In panel (c), interlayer coupling e^{-2qd} is set to 0.86.

instabilities in the HD regime is located between $\beta^-_{\rm th}$ and $\beta^+_{\rm th}$,

$$\beta^{\pm}_{\rm th} = \frac{v_0}{\sqrt{2}}\sqrt{\frac{q^2v_0^2+2\omega_p^2(1\pm e^{-|q|d})}{q^2v_0^2+\omega_p^2(1\pm e^{-|q|d})}}, \tag{15}$$

where $\omega_p = (2\pi ne^2|q|/m)^{1/2}$ is the plasma frequency in an isolated graphene layer. Note that plus and minus signs in Eq. (15) correspond to upper and lower critical velocities, not

to optical and acoustic modes. The optical mode is always stable. $\beta_{\rm th}^{-}$ has a natural lower bound $v_0/\sqrt{2}$ that coincides with sound velocity. Interestingly, the threshold velocity weakly depends on carrier density as far as layers are closely bound ($qd \ll 1$).

The growth rate of unstable modes is going down as the e-e collision frequency is reduced, shown in Fig. 3(b). In the weak HD regime, $ql_{\rm ee} \lesssim 1$, the reduced growth rate can be attributed to increased viscous damping. However, outside of the hydrodynamic domain $ql_{\rm ee} \gtrsim 1$, the instabilities do not reappear as the velocity of acoustic modes is forced to lie above the velocity of carrier drift.

The full stability diagram of the counterstreaming double-layer system is calculated in Fig. 3(c): The values of drift velocity and e-e collision frequency above the threshold lines correspond to unstable modes. Remarkably, the e-e collision frequency in the dispersion relation appears scaled to qv_0. It implies that the only parameter governing the transition between HD and ballistic regimes is the Knudsen number $qv_0/\gamma_{\rm ee} = ql_{\rm ee}$, where $l_{\rm ee}$ is an electron free path with respect to e-e collisions. As a result, instabilities can always be observed in clean systems of sufficiently large length.

V. DISTRIBUTED-FEEDBACK PLASMON LASING IN CURRENT-BIASED GRAPHENE

A highly resonant instability leading to electromagnetic emission can be observed in graphene with a conducting substrate covered by a metal grating. Such a setup is commonly used for spectroscopy of plasmon resonance in 2D electron systems [45]. The reflectance spectrum of such setup is calculated using the formalism of Refs. [46,47] with graphene conductivity found from Eqs. (4) and (5) as a building block (Supplemental Material, Sec. V [35]).

The electromagnetic response of grating-coupled graphene differs for hydrodynamic and ballistic regimes already in the absence of dc current. Namely, the frequencies of plasmonic dips are reduced by e-e collisions (Fig. 4). When passing direct current in 2DES, the absorption peak is split by the Doppler effect [28,46,47]. With increasing current, the distinctions between HD and ballistic regimes become more drastic.

The Doppler shift in the ballistic regime is so weak and the singular nonlocal response at $\omega = qv_0$ is so strong that the plasmon frequency is almost unaffected by current [shown in Fig. 3(b). On the contrary, the plasmon frequency in the hydrodynamic regime passes to zero frequency unimpededly [Fig. 4(a). At higher current, the resonant frequency grows again, but the reflection coefficient exceeds unity. The negative absorption is associated with the generation of evanescent waves by the grating that falls into the negative conductivity domain of 2DES; the effect is enhanced if frequency corresponds to plasmon resonance.

The negativity of absorption at high drift velocities is further elucidated by writing the power density Q dissipated in the graphene layer

$$Q = \sum_{\mathbf{G}_n = 2\pi n/a} 2{\rm Re}\sigma_{\mathbf{G}_n\omega} \left|\mathbf{E}_{\mathbf{G}_n\omega}\right|^2, \qquad (16)$$

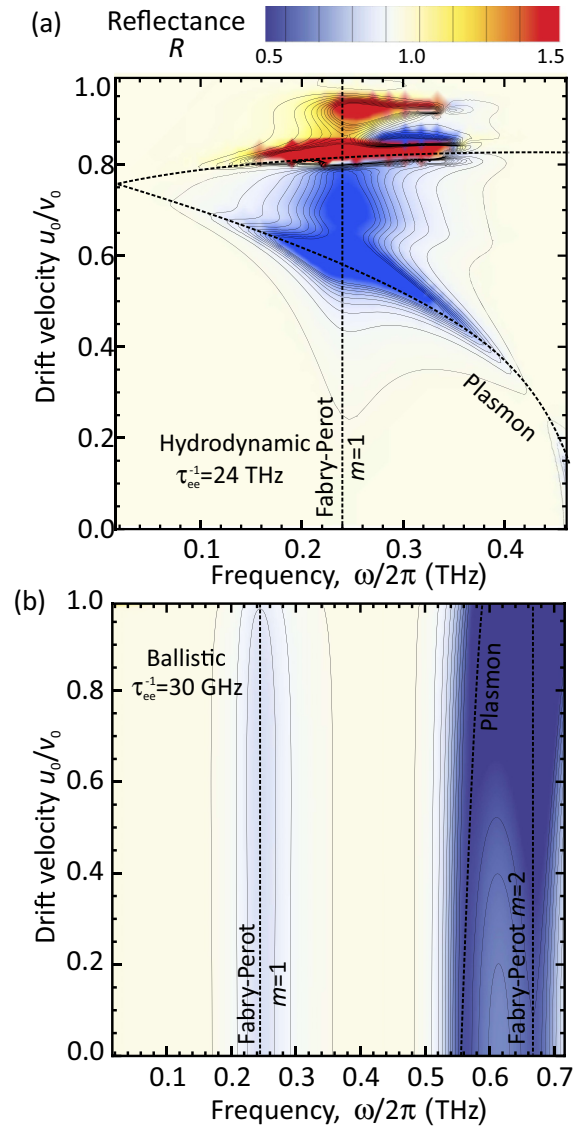

FIG. 4. Evolution of reflectance spectra of graphene covered by plasmonic grating with increasing carrier drift velocity in the hydrodynamic (a) and ballistic (b) regimes. Bright regions correspond to the excitation of plasmon and Fabry-Perot modes. At large drift velocity, plasmon-enhanced absorption ($R < 1$) turns to plasmon enhanced amplification ($R > 1$). The reflection coefficient further diverges at the crossing of Fabry-Perot and plasmon resonance. Parameters: $\mu = 50$ meV, $d = 3$ nm, $D = 100$ μm, $\kappa = 12$, grating period is $a = 2$ μm, width of metal gate $W = a/2 = 1$ μm.

where the summation is performed over all diffraction orders n, a being the grating period. The real part of conductivity is negative in the Cerenkov domain $G_n > \omega/u_0$ and positive otherwise. In a nonresonant system, the high-order diffraction harmonics prone to Cerenkov amplification are exponentially suppressed due to the evanescent character of fields with $n > 1$. Therefore, dissipative terms with ${\rm Re}\sigma_{\mathbf{G}_n\omega} > 0$ dominate the sum (16) in the absence of resonances. Under conditions of nth order plasmon resonance, the electric field $\mathbf{E}_{\mathbf{G}_n\omega}$ grows, which can lead to the negativity of full power Q provided ${\rm Re}\sigma_{\mathbf{G}_n\omega} < 0$.

Further enhancement of both absorption and amplification occurs if the distance D between 2DES and the conducting substrate satisfies the antireflection condition, $D = \lambda_0/4\sqrt{\kappa}$, where κ is the background dielectric constant. The effect occurs once the eigenfrequency of the Fabry-Perot cavity formed in the vertical direction coincides with the frequency of plasmon. The interaction of plasmon at high current with Fabry-Perot mode leads to a divergent reflection coefficient. The divergence implies that such a mode can grow without external stimulus until it is stabilized by nonlinear effects, as it occurs in the distributed feedback lasers.

VI. DISCUSSION AND CONCLUSIONS

We now argue that Cerenkov-type plasmon instability in Dirac materials in the HD regime and its absence in the ballistic regime are linked to a singular structure of conductivity $\sigma(q, \omega)$ independent of particular dielectric environment. These considerations should be applicable both to 2D and 3D Dirac materials, where conductivity has square root and log singularities [48], respectively, at $\omega = qv_0$.

The TM plasmon modes of arbitrary structure exist in the domain of the positive imaginary part of conductivity $\mathrm{Im}\sigma(q, \omega) > 0$ which, in the ballistic regime, lies above the singularity, $\omega > qv_0$ [Fig. 1(c). The Cerenkov domain $\omega < qu_0$ lies below the singularity. The position of the singularity is insensitive to carrier drift. Therefore, one cannot thread the plasmon modes through the singularity by a continuous change of parameter u_0. This, however, becomes possible in the hydrodynamic regime ($\mathrm{Kn} \ll 1$), where the singularity is removed from the real frequency axis due to strong e-e collisions. These arguments do not apply to combinations of Dirac and parabolic-band materials (e.g., graphene parallel to bulk collisionless plasma), where joint plasmon modes can exist at $\omega < qu_0$.

The predicted effects can be readily tested experimentally. The anomalous Doppler shifts of plasmons in graphene can be measured with Raman spectroscopy [49]. The plasmon instabilities can result in oscillatory current regimes [50] and emission of terahertz radiation. Such emission can be distinguished from hot-plasmonic emission [51] by the presence of well-defined threshold current [52]. Reflectance spectroscopy of grating-gated 2DES is another convenient tool to study Doppler shift and wave amplification [53].

ACKNOWLEDGMENTS

This work was supported by the grants 18-37-20058/18 and 16-29-03402/18 of the Russian Foundation for Basic Research. The author thanks Denis Fateev for helpful discussions and Mikhail K. Maslov for assistance in the early stages of the work.

[1] E. Lifshits and L. Pitaevskii, *Physical Kinetics (Course of Theoretical Physics)* (Pergamon Press, Oxford, 1981).
[2] P. J. W. Moll, P. Kushwaha, N. Nandi, B. Schmidt, and A. P. Mackenzie, Science **351**, 1061 (2016).
[3] J. Gooth, F. Menges, N. Kumar, V. Süß, C. Shekhar, Y. Sun, U. Drechsler, R. Zierold, C. Felser, and B. Gotsmann, Nat. Commun. **9**, 4093 (2018).
[4] A. D. Levin, G. M. Gusev, E. V. Levinson, Z. D. Kvon, and A. K. Bakarov, Phys. Rev. B **97**, 245308 (2018).
[5] D. A. Bandurin, I. Torre, R. K. Kumar, M. Ben Shalom, A. Tomadin, A. Principi, G. H. Auton, E. Khestanova, K. S. Novoselov, I. V. Grigorieva, L. A. Ponomarenko, A. K. Geim, and M. Polini, Science **351**, 1055 (2016).
[6] R. Krishna Kumar, D. Bandurin, F. Pellegrino, Y. Cao, A. Principi, H. Guo, G. Auton, M. B. Shalom, L. A. Ponomarenko, G. Falkovich *et al.*, Nat. Phys. **13**, 1182 (2017).
[7] J. A. Sulpizio, L. Ella, A. Rozen, J. Birkbeck, D. J. Perello, D. Dutta, M. Ben-Shalom, T. Taniguchi, K. Watanabe, T. Holder *et al.*, arXiv:1905.11662.
[8] D. Y. H. Ho, I. Yudhistira, N. Chakraborty, and S. Adam, Phys. Rev. B **97**, 121404(R) (2018).
[9] A. S. Mayorov, R. V. Gorbachev, S. V. Morozov, L. Britnell, R. Jalil, L. A. Ponomarenko, P. Blake, K. S. Novoselov, K. Watanabe, T. Taniguchi *et al.*, Nano Lett. **11**, 2396 (2011).
[10] D. A. Bandurin, A. V. Shytov, L. S. Levitov, R. K. Kumar, A. I. Berdyugin, M. B. Shalom, I. V. Grigorieva, A. K. Geim, and G. Falkovich, Nat. Commun. **9**, 4533 (2018).
[11] A. Shytov, J. F. Kong, G. Falkovich, and L. Levitov, Phys. Rev. Lett. **121**, 176805 (2018).
[12] P. Gallagher, C.-S. Yang, T. Lyu, F. Tian, R. Kou, H. Zhang, K. Watanabe, T. Taniguchi, and F. Wang, Science **364**, 158 (2019).
[13] P. L. Bhatnagar, E. P. Gross, and M. Krook, Phys. Rev. **94**, 511 (1954).
[14] A. A. Abrikosov and I. M. Khalatnikov, Rep. Prog. Phys. **22**, 329 (1959).
[15] S. Conti and G. Vignale, Phys. Rev. B **60**, 7966 (1999).
[16] D. Svintsov, Phys. Rev. B **97**, 121405(R) (2018).
[17] J. Crossno, J. K. Shi, K. Wang, X. Liu, A. Harzheim, A. Lucas, S. Sachdev, P. Kim, T. Taniguchi, K. Watanabe, T. A. Ohki, and K. C. Fong, Science **351**, 1058 (2016).
[18] V. Ryzhii, Jpn. J. Appl. Phys. **45**, L923 (2006).
[19] M. B. Lundeberg, Y. Gao, R. Asgari, C. Tan, B. Van Duppen, M. Autore, P. Alonso-González, A. Woessner, K. Watanabe, T. Taniguchi, R. Hillenbrand, J. Hone, M. Polini, and F. H. L. Koppens, Science **357**, 187 (2017).
[20] D. Svintsov, V. Vyurkov, S. Yurchenko, T. Otsuji, and V. Ryzhii, J. Appl. Phys. **111**, 083715 (2012).
[21] G. Gumbs, A. Iurov, D. Huang, and W. Pan, J. Appl. Phys. **118**, 054303 (2015).
[22] T. A. Morgado and M. G. Silveirinha, Phys. Rev. Lett. **119**, 133901 (2017).
[23] L. S. Levitov, A. V. Shtyk, and M. V. Feigelman, Phys. Rev. B **88**, 235403 (2013).
[24] D. Svintsov, V. Vyurkov, V. Ryzhii, and T. Otsuji, Phys. Rev. B **88**, 245444 (2013).
[25] D. S. Borgnia, T. V. Phan, and L. S. Levitov, arXiv:1512.09044.
[26] D. Svintsov and V. Ryzhii, Phys. Rev. Lett. **123**, 219401 (2019).

[27] B. V. Duppen, A. Tomadin, A. N. Grigorenko, and M. Polini, 2D Materials **3**, 015011 (2016).
[28] T. Wenger, G. Viola, J. Kinaret, M. Fogelström, and P. Tassin, Phys. Rev. B **97**, 085419 (2018).
[29] M. Sabbaghi, H.-W. Lee, T. Stauber, and K. S. Kim, Phys. Rev. B **92**, 195429 (2015).
[30] The instability found in Ref. [29] is related to current-induced interband population inversion which can be obtained near the charge neutrality point. Here, we consider only the intraband plasmon emission.
[31] D. J. Bergman and M. I. Stockman, Phys. Rev. Lett. **90**, 027402 (2003).
[32] M. Krasheninnikov and A. Chaplik, Sov. Phys. JETP **52**, 279 (1980).
[33] D. Bohm and E. P. Gross, Phys. Rev. **75**, 1864 (1949).
[34] G. S. Atwal and N. W. Ashcroft, Phys. Rev. B **65**, 115109 (2002).
[35] See Supplemental Material at http://link.aps.org/supplemental/10.1103/PhysRevB.100.195428 for (1) derivation of nonlinear hydrodynamic equations for 2D Dirac electrons, (2) detailed consideration of hydrodynamic-to-ballistic crossover for drifting Dirac electrons, (3) analytical evaluation of spatially dispersive integrals, (4) detailed analysis of instabilities in double-layer graphene, and (5) description of numerical algorithm for solving the diffraction problem for a 2D electron system with a grating.
[36] S. Kukhtaruk, V. Kochelap, V. Sokolov, and K. Kim, Physica E **79**, 26 (2016).
[37] U. Briskot, M. Schütt, I. V. Gornyi, M. Titov, B. N. Narozhny, and A. D. Mirlin, Phys. Rev. B **92**, 115426 (2015).
[38] P. Halevi, Phys. Rev. B **51**, 7497 (1995).
[39] V. Fessatidis and H. L. Cui, Phys. Rev. B **43**, 11725 (1991).
[40] A. Eguiluz and J. J. Quinn, Phys. Rev. B **14**, 1347 (1976).
[41] E. H. Hwang and S. Das Sarma, Phys. Rev. B **75**, 205418 (2007).
[42] B. Wunsch, T. Stauber, F. Sols, and F. Guinea, New J. Phys. **8**, 318 (2006).
[43] K. Moors, T. L. Schmidt, and O. Kashuba, arXiv:1905.01247.
[44] R. E. V. Profumo, R. Asgari, M. Polini, and A. H. MacDonald, Phys. Rev. B **85**, 085443 (2012).
[45] S. J. Allen, D. C. Tsui, and R. A. Logan, Phys. Rev. Lett. **38**, 980 (1977).
[46] S. A. Mikhailov, Phys. Rev. B **58**, 1517 (1998).
[47] O. R. Matov, O. V. Polischuk, and V. V. Popov, Int. J. Infrared and Millim. Waves **14**, 1455 (1993).
[48] M. Lv and S.-C. Zhang, Int. J. Mod. Phys. B **27**, 1350177 (2013).
[49] L. C. Ó. Súilleabháin, H. P. Hughes, A. C. Churchill, D. A. Ritchie, M. P. Grimshaw, and G. A. C. Jones, J. Appl. Phys. **76**, 1701 (1994).
[50] Z. S. Gribnikov, N. Z. Vagidov, and V. V. Mitin, J. Appl. Phys. **88**, 6736 (2000).
[51] D. Tsui, E. Gornik, and R. Logan, Solid State Commun. **35**, 875 (1980).
[52] A. El Fatimy, N. Dyakonova, Y. Meziani, T. Otsuji, W. Knap, S. Vandenbrouk, K. Madjour, D. Théron, C. Gaquiere, M. A. Poisson, S. Delage, P. Prystawko, and C. Skierbiszewski, J. Appl. Phys. **107**, 024504 (2010).
[53] S. Boubanga-Tombet, D. Yadav, W. Knap, V. V. Popov, and T. Otsuji, arXiv:1801.04518.